

# Detection of glycolaldehyde towards the solar-type protostar NGC 1333 IRAS2A<sup>★</sup>

A. Coutens<sup>1</sup>, M. V. Persson<sup>2</sup>, J. K. Jørgensen<sup>1</sup>, S. F. Wampfler<sup>1</sup>, and J. M. Lykke<sup>1</sup>

<sup>1</sup> Centre for Star and Planet Formation, Niels Bohr Institute and Natural History Museum of Denmark, University of Copenhagen, Øster Voldgade 5-7, DK-1350 Copenhagen K, Denmark  
e-mail: acoutens@nbi.dk

<sup>2</sup> Leiden Observatory, Leiden University, PO Box 9513, 2300 RA Leiden, The Netherlands

Received xxx; accepted xxx

## ABSTRACT

Glycolaldehyde is a key molecule in the formation of biologically relevant molecules such as ribose. We report its detection with the Plateau de Bure interferometer towards the Class 0 young stellar object NGC 1333 IRAS2A, which is only the second solar-type protostar for which this prebiotic molecule is detected. Local thermodynamic equilibrium analyses of glycolaldehyde, ethylene glycol (the reduced alcohol of glycolaldehyde) and methyl formate (the most abundant isomer of glycolaldehyde) were carried out. The relative abundance of ethylene glycol to glycolaldehyde is found to be  $\sim 5$  – higher than in the Class 0 source IRAS 16293-2422 ( $\sim 1$ ), but comparable to the lower limits derived in comets ( $\geq 3$ –6). The different ethylene glycol-to-glycolaldehyde ratios in the two protostars could be related to different  $\text{CH}_3\text{OH}:\text{CO}$  compositions of the icy grain mantles. In particular, a more efficient hydrogenation on the grains in NGC 1333 IRAS2A would favor the formation of both methanol and ethylene glycol. In conclusion, it is possible that, like NGC 1333 IRAS2A, other low-mass protostars show high ethylene glycol-to-glycolaldehyde abundance ratios. The cometary ratios could consequently be inherited from earlier stages of star formation, if the young Sun experienced conditions similar to NGC 1333 IRAS2A.

**Key words.** astrochemistry – astrobiology – stars: formation – stars: protostars – ISM: molecules – ISM: individual object (NGC 1333 IRAS2A)

## 1. Introduction

The inner regions of low-mass protostars are known to harbor a rich complex organic chemistry characterized by the presence of molecules such as methyl formate ( $\text{CH}_3\text{OCHO}$ ), dimethyl ether ( $\text{CH}_3\text{OCH}_3$ ), and ethyl cyanide ( $\text{C}_2\text{H}_5\text{CN}$ ) (e.g., Cazaux et al. 2003; Bottinelli et al. 2004a; Bisschop et al. 2008). To differentiate them from the hot cores present in high-mass star-forming regions, they were called hot corinos (Ceccarelli 2004; Bottinelli et al. 2004b). These complex organic molecules are thought to be efficiently formed on grains and then released into the gas phase in the hot corino by thermal desorption (e.g., Garrod et al. 2008; Herbst & van Dishoeck 2009). Some of these complex organic molecules are particularly interesting because of their supposed role in the emergence of life. Indeed, the detection of so called prebiotic molecules in low-mass star-forming regions indicates that they can form early during the star formation process and thereby be available for possible later incorporation into solar system bodies, e.g., comets.

Glycolaldehyde ( $\text{CH}_2\text{OHCHO}$ ) is one of these prebiotic molecules: it is a simple sugar-like molecule and under Earth-like conditions the first product in the formose reaction leading to the formation of ribose, an essential constituent of ribonucleic acid (RNA) (e.g., Zubay & Mui 2001; Jalbout et al. 2007). Glycolaldehyde was first detected towards the Galactic center (Sgr B2(N); Hollis et al. 2000, 2001, 2004; Halfen et al. 2006; Bel-

loche et al. 2013; molecular clouds: Requena-Torres et al. 2008). Later it was shown to be present in the high mass star-forming region G31.41+0.31 (Beltrán et al. 2009), in the intermediate mass protostar NGC 7129 FIRS 2 (Fuente et al. 2014), and even in the hot corinos of the Class 0 protostellar binary, IRAS 16293-2422 (hereafter IRAS16293, Jørgensen et al. 2012). This indicates that this molecule can be synthesized relatively early in the environments of solar-type protostars. Furthermore, glycolaldehyde can easily survive during impact delivery to planetary bodies, and impacts can even facilitate the formation of even more complex molecules (McCaffrey et al. 2014).

Similarly to other complex organic molecules, the formation of glycolaldehyde is thought to occur on grains. In particular, a gas phase formation was excluded by Woods et al. (2012, 2013), as the produced abundances are too low compared with the observations. Several grain surface formation pathways were proposed in the literature. Woods et al. (2012) modeled their efficiency and showed that the formation by the reaction  $\text{CH}_3\text{OH} + \text{HCO}$  would be very efficient, but that, from chemical considerations,  $\text{H}_3\text{CO} + \text{HCO}$  could be more feasible. Another probably efficient way to form glycolaldehyde would be through HCO dimerization ( $\text{HCO} + \text{HCO} \rightarrow \text{HOCCOH}$ ) followed by two successive hydrogenations (Woods et al. 2013). A recent experimental study based on surface hydrogenations of CO seems to confirm this pathway (Fedoseev et al. submitted).

A related species to this prebiotic molecule is ethylene glycol ( $(\text{CH}_2\text{OH})_2$ ). More commonly known as antifreeze, it is the reduced alcohol of glycolaldehyde. This molecule was tentatively detected towards IRAS16293 with one line of the  $\text{gGg}'$

<sup>★</sup> Based on observations carried out with the IRAM Plateau de Bure Interferometer. IRAM is supported by INSU/CNRS (France), MPG (Germany) and IGN (Spain).

conformer (Jørgensen et al. 2012). Interestingly, the aGg' conformer of ethylene glycol (the conformer of lowest energy) was detected in three comets, Hale-Bopp, Lemmon, and Lovejoy, while glycolaldehyde was not, leading to a lower limit of 3–6 for the  $(\text{CH}_2\text{OH})_2/\text{CH}_2\text{OHCHO}$  abundance ratio (Crovisier et al. 2004; Biver et al. 2014). Ethylene glycol was also detected in the Murchison and Murray carbonaceous meteorites, while the presence of aldehyde sugars have not been reported yet (Cooper et al. 2001).

NGC 1333 IRAS2A (hereafter IRAS2A) is another of these famous hot corinos. In particular, methyl formate, the most abundant isomer of glycolaldehyde, was detected towards this source by Jørgensen et al. (2005a) and Bottinelli et al. (2007). More recently, ethylene glycol was detected in the framework of the CALYPSO program carried out with the IRAM Plateau de Bure Interferometer (PdBI) by Maury et al. (2014). We here report the detection of glycolaldehyde towards the same low-mass protostar, and present an analysis of the relative abundances of these three species.

## 2. Observations

This work is based on several separate programs carrying out observations of the solar-type protostar IRAS2A with the PdBI. Four spectral ranges (84.9–88.5, 223.5–227.1, 240.2–243.8, and 315.5–319.1 GHz) were covered with the WIDEX correlator at a spectral resolution of 1.95 MHz ( $dv = 6.8 \text{ km s}^{-1}$  at 86 GHz,  $dv = 2.6 \text{ km s}^{-1}$  at 225 GHz,  $dv = 2.4 \text{ km s}^{-1}$  at 242 GHz,  $dv = 1.8 \text{ km s}^{-1}$  at 317 GHz) and reduced with the GILDAS<sup>1</sup> software. The synthesized beam sizes obtained with natural weighting are about  $3.0'' \times 3.0''$  at 86 GHz,  $1.2'' \times 1.0''$  at 225 GHz,  $1.4'' \times 1.0''$  at 242 GHz, and  $0.9'' \times 0.8''$  at 317 GHz. The dust continuum fluxes at 0.9 and 1.3 mm are consistent with previous measurements (e.g., Jørgensen et al. 2007; Persson et al. 2012). The absolute calibration uncertainty for each dataset is about 20%. Additional information about the observations and their reduction can be found in Coutens et al. (2014) and Persson et al. (2014). The 3mm data are from Wampfler (priv. comm.).

Using the CASSIS<sup>2</sup> software, we detected 8 lines of glycolaldehyde, 31 lines of the aGg' conformer of ethylene glycol, and 26 lines of methyl formate (see Table 1). The glycolaldehyde and methyl formate transitions are taken from the JPL spectroscopic database (Pickett et al. 1998), while the ethylene glycol transitions are from the CDMS catalogue (Müller et al. 2001, 2005). The predictions are based on experimental data from Butler et al. (2001), Widicus Weaver et al. (2005) and Carroll et al. (2010) for glycolaldehyde, Christen et al. (1995) and Christen & Müller (2003) for ethylene glycol, and Ilyushin et al. (2009) for methyl formate. The frequencies of five of the detected glycolaldehyde lines were directly measured in the laboratory (Butler et al. 2001). Some of the lines result from a blending of several transitions of the same species. The lines that are strongly blended with other species are not listed in Table 1. All three species are emitted very compactly at the position of the continuum peak ( $\alpha_{2000}=03^{\text{h}}28^{\text{m}}55^{\text{s}}.57$ ,  $\delta_{2000}=31^{\circ}14'37''.1$ ). The angular sizes obtained with a circular Gaussian fit in the  $(u,v)$  plane vary from a point source to a maximum of  $1''$  depending on the transition. The line fluxes listed in Table 1 were measured at the continuum peak position with the CASSIS software using a Gaussian fitting method (Levenberg-Marquardt algorithm). The lines that are contaminated in the wings by other transitions are con-

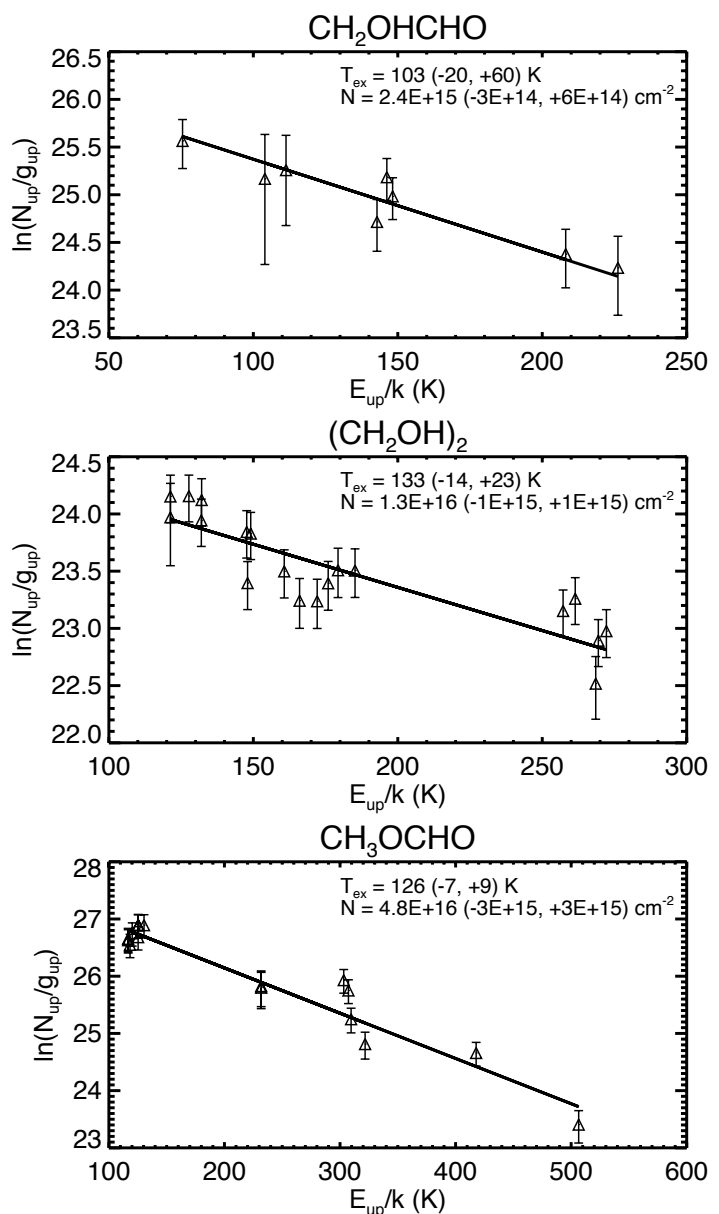


**Fig. 1.** Rotational diagrams for glycolaldehyde, ethylene glycol, and methyl formate.

sequently fitted with a sum of Gaussians. We carefully checked that the derived full widths at half maximum ( $FWHM$ ) are consistent with the other line measurements. The average  $FWHM$  is about  $4.5 \text{ km s}^{-1}$  at 317 GHz, and  $5.0 \text{ km s}^{-1}$  at 225 and 242 GHz. The widths of the methyl formate lines at 87 GHz are quite broad ( $\sim 12 \text{ km s}^{-1}$ ). It is consequently difficult to completely exclude an extra flux contribution from other species. The variation of  $FWHM$  with the frequency can be explained by the spectral resolution of the observations that decreases towards the lower frequencies.

## 3. Results

We carried out a local thermodynamic equilibrium analysis of the three species through the rotational diagram method (Goldsmith & Langer 1999). We consider that the lines are emitted in a region of  $0.5''$  size, which is the average size derived for

<sup>1</sup> <http://www.iram.fr/IRAMFR/GILDAS/>

<sup>2</sup> <http://cassis.iram.omp.eu>

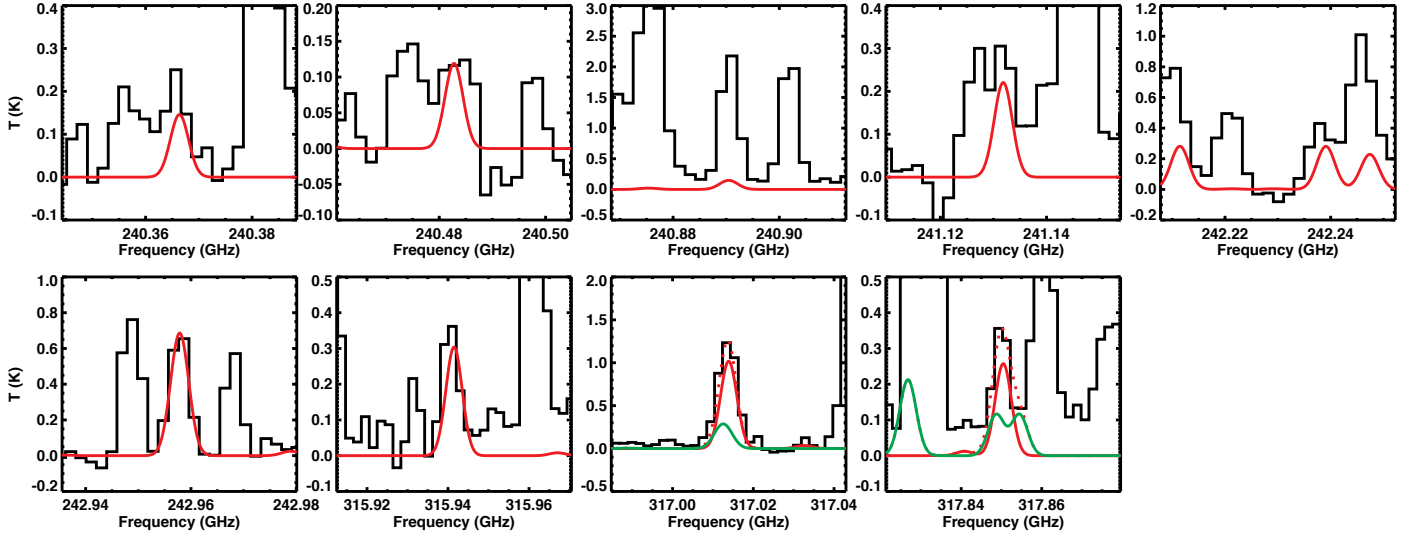


**Fig. 2.** Observed lines of  $\text{CH}_2\text{OHCHO}$  towards the protostar NGC 1333 IRAS2A (in black). The best-fit model for  $\text{CH}_2\text{OHCHO}$  (see Table 2) is shown in red solid lines. The line in the third upper panel is blended with an unidentified species. The contribution of the  $\text{CH}_3\text{OCHO}$  lines is indicated with green lines, and the model including both  $\text{CH}_2\text{OHCHO}$  and  $\text{CH}_3\text{OCHO}$  can be seen in red dotted lines.

the methyl formate lines when fitting circular gaussians in the  $(u,v)$  plane (see also Maury et al. 2014). It is also similar to what we found for deuterated water (Coutens et al. 2014). It also corresponds to the expected size of the region where the temperature increases above  $\sim 100$  K according to dust radiation transfer models of the envelope (Jørgensen et al. 2002) and where the complex molecules and deuterated water should sublime from the grains. The line fluxes that result from a combination of several transitions of the same species are used in the rotational diagrams, unless the transitions have different  $E_{\text{up}}$  values. For glycolaldehyde, we include two lines slightly blended with some methyl formate transitions after subtraction of the predicted flux contribution from methyl formate. As the best-fit model for methyl formate reproduces extremely well the observations, the final fluxes of the glycolaldehyde lines can be trusted, which is also confirmed by their alignment with the other points in the rotational diagram of glycolaldehyde (see upper panel in Figure 1). Assuming a source size of  $0.5''$ , we derive column densities (with  $1\sigma$  uncertainties) of  $2.4^{+0.6}_{-0.3} \times 10^{15} \text{ cm}^{-2}$ ,  $1.3^{+0.1}_{-0.1} \times 10^{16} \text{ cm}^{-2}$ , and  $4.8^{+0.3}_{-0.3} \times 10^{16} \text{ cm}^{-2}$ , and excitation temperatures of  $103^{+60}_{-20}$  K,  $133^{+23}_{-14}$  K, and  $126^{+9}_{-7}$  K for glycolaldehyde, ethylene glycol, and methyl formate, respectively. Within the uncertainty range, the excitation temperature seems to be similar between the three species ( $\sim 130$  K), which is consistent if the three species arise from a same region. We checked, for each species, that there is no line flux overproduced by the model anywhere in the four datasets. In the case of ethylene glycol, the model shows an overproduced flux for some transitions, especially the lines (240.778, 241.545, 241.860, and 316.444 GHz) that correspond to the four lower points in the rotational diagram (see middle panel in Figure 1). A model with a column density of  $1.1 \times 10^{16} \text{ cm}^{-2}$  would be sufficient to produce line fluxes consistent with these observations. Table 2 summarizes the parameters used for the line modeling of the three species that can be seen in Figures 2, 3, and 4. According to these models, all lines are optically thin ( $\tau \leq 0.1$ ).

Although no other species than glycolaldehyde is found at a frequency of 240890.5 MHz, the line ( $E_{\text{up}} = 52$  K) is probably

**Table 2.** Parameters used to compute the synthetic spectra of glycolaldehyde, ethylene glycol, and methyl formate.

Molecule	Source size ( $''$ )	$T_{\text{ex}}$ (K)	$N$ ( $\text{cm}^{-2}$ )	$v_{\text{LSR}}$ ( $\text{km s}^{-1}$ )
$\text{CH}_2\text{OHCHO}$	0.5	130	$2.4 \times 10^{15}$	7.0
$\text{aGg}'-(\text{CH}_2\text{OH})_2$	0.5	130	$1.1 \times 10^{16}$	7.0
$\text{CH}_3\text{OCHO}$	0.5	130	$4.8 \times 10^{16}$	7.0

**Notes.** The FWHM used for the line modeling are 4.5, 5.0, 5.0, and  $7.0 \text{ km s}^{-1}$  for the data at 317, 242, 225, and 86 GHz, respectively.

blended with an unidentified species: the predicted flux is completely underproduced with respect to the observations, and it cannot be due to a different excitation in the cold gas, as a line of glycolaldehyde at 243232.21 MHz ( $E_{\text{up}} = 47$  K) – blended with a bright  $\text{CH}_2\text{DOH}$  line in the red-shifted part of the spectrum and also potentially blended with a  $\text{DCOOH}$  line ( $E_{\text{up}} = 106$  K,  $A_{ij} = 1.35 \times 10^{-4} \text{ s}^{-1}$ ) – would have a higher flux inconsistent with the observed one.

#### 4. Discussion

The relative abundances of the three species are derived from the column densities in Table 2 and compared with other star-forming regions and comets in Table 3. The  $(\text{CH}_2\text{OH})_2/\text{CH}_2\text{OHCHO}$  abundance ratio of  $\sim 0.3$ – $0.5$  previously derived in IRAS16293 by Jørgensen et al. (2012) was revised. Indeed, the assignment in Jørgensen et al. (2012) was based on only one line of the  $\text{gGg}'$  conformer of ethylene glycol about  $200 \text{ cm}^{-1}$  ( $\sim 290$  K, Müller & Christen 2004) above the lowest-energy  $\text{aGg}'$  conformer – and thus tentative. An analysis from observations of 6 transitions of the lower energy conformer from ALMA Cycle 1 observations at 3 mm (4 spectral windows at 89.48–89.73, 92.77–93.03, 102.48–102.73 and 103.18–103.42 GHz; Jørgensen et al. in prep.) results in a higher ethylene glycol-to-glycolaldehyde abundance ratio of  $1.0 \pm 0.3$ .

**Table 3.**  $(\text{CH}_2\text{OH})_2/\text{CH}_2\text{OHCHO}$ ,  $\text{CH}_3\text{OCHO}/\text{CH}_2\text{OHCHO}$ , and  $\text{CH}_3\text{OCHO}/(\text{CH}_2\text{OH})_2$  column density ratios determined in different objects.

Source	$(\text{CH}_2\text{OH})_2/\text{CH}_2\text{OHCHO}^a$	$\text{CH}_3\text{OCHO}/\text{CH}_2\text{OHCHO}$	$\text{CH}_3\text{OCHO}/(\text{CH}_2\text{OH})_2^a$	References
Class 0 protostars				
NGC 1333 IRAS2A	$\sim 5$	$\sim 20$	$\sim 4$	1
IRAS 16293-2422	$\sim 1$	$\sim 13$	$\sim 13$	2
Comets				
C/1995 O1 (Hale-Bopp)	$\geq 6$	$\geq 2$	$\sim 0.3$	3
C/2012 F6 (Lemmon)	$\geq 3$	...	$\leq 0.7$	4
C/2013 R1 (Lovejoy)	$\geq 5$	...	$\leq 0.6$	4
High- and intermediate-mass star forming regions				
Sgr B2(N)	$0.7\text{--}2.2^b$	$\sim 52^c$	$\sim 30$	5, 6, 7
G34.41+0.31	...	$\leq 34$	...	8
NGC7129 FIRS2	$\sim 2$	$\sim 40$	$\sim 20$	9
Molecular clouds in the Central Molecular Zone				
G-0.02, G-0.11, and G+0.693	$\sim 1.2\text{--}1.6$	$\sim 3.3\text{--}5.2$	$\sim 2.5\text{--}4.3$	10

**Notes.** <sup>(a)</sup>  $(\text{CH}_2\text{OH})_2$  refers to the aGg' conformer. <sup>(b)</sup> Large scale emission. <sup>(c)</sup> Hot core emission.

**References.** 1) this study, 2) Jørgensen et al. (2012, in prep.), 3) Crovisier et al. (2004), 4) Biver et al. (2014), 5) Hollis et al. (2001), 6) Hollis et al. (2002), 7) Belloche et al. (2013), 8) Beltrán et al. (2009), 9) Fuente et al. (2014), 10) Requena-Torres et al. (2008).

This new estimate is consistent with the ratio expected between the aGg' and gGg' conformers under thermal equilibrium conditions at 300 K, the excitation temperature of glycolaldehyde derived in IRAS16293 (Jørgensen et al. 2012). The  $(\text{CH}_2\text{OH})_2/\text{CH}_2\text{OHCHO}$  abundance ratio in IRAS2A is estimated at  $5.5 \pm 1.0$  if we consider the column densities derived from the rotational diagrams. It is however slightly lower (4.6) if we use the column density of ethylene glycol of  $1.1 \times 10^{16} \text{ cm}^{-2}$  that does not overproduce the peak intensities of a few lines (see Fig. 3). The  $(\text{CH}_2\text{OH})_2/\text{CH}_2\text{OHCHO}$  abundance ratio is consequently a factor  $\sim 5$  higher than in the Class 0 protostar IRAS16293. It is also higher than in the other star-forming regions (see Table 3), but comparable to the lower limits derived in comets ( $\geq 3\text{--}6$ ). This indicates that the glycolaldehyde chemistry may vary among hot corinos in general. It is possible that, like IRAS2A, other very young low-mass protostars show high  $(\text{CH}_2\text{OH})_2/\text{CH}_2\text{OHCHO}$  abundance ratios, in agreement with the cometary values. The  $\text{CH}_3\text{OCHO}/\text{CH}_2\text{OHCHO}$  column density ratio found in IRAS2A ( $\sim 20$ ) ranges between the values derived in the molecular clouds from the Galactic Center ( $\sim 3.3\text{--}5.2$ ) and the high-mass star-forming regions ( $\sim 40\text{--}52$ ). A lower limit of 2 was derived for the Hale-Bopp comet.

In contrast to IRAS16293, the  $(\text{CH}_2\text{OH})_2/\text{CH}_2\text{OHCHO}$  abundance ratio in IRAS2A is comparable to the lower limits in comets. To explain these different abundance ratios in IRAS2A and IRAS16293, two scenarios are possible: either the  $(\text{CH}_2\text{OH})_2/\text{CH}_2\text{OHCHO}$  ratio is similar in the grain mantles of low-mass protostars and it evolves in the gas phase after the sublimation of the molecules in the hot corinos, or this ratio was already different in the grain mantles of the two protostars.

In the first scenario, if we assume that the  $(\text{CH}_2\text{OH})_2/\text{CH}_2\text{OHCHO}$  increases until it reaches the cometary value, it would mean that glycolaldehyde can easily be destroyed in the gas phase of the warm inner regions. Another possibility would be that ethylene glycol can form efficiently in the gas phase, but complex organic molecules are generally difficult to form with high abundances in the gas phase. If the evaporation temperature of ethylene glycol is higher than glycolaldehyde, as assumed in the chemical model of Garrod (2013), ethylene glycol would desorb later than glycolaldehyde and the

$(\text{CH}_2\text{OH})_2/\text{CH}_2\text{OHCHO}$  abundance ratio would consequently increase with time (until the two molecules have completely desorbed). This chemical model however predicts an abundance of glycolaldehyde significantly higher than those of ethylene glycol and methyl formate, which is inconsistent with the ratios derived in IRAS2A. More theoretical and experimental work would be needed to make the case that these hypotheses are plausible.

In contrast, experimental studies based on irradiation of ices show that the second scenario is likely. Such studies show that glycolaldehyde, ethylene glycol, and methyl formate can be synthesized by irradiation of pure or mixed methanol ( $\text{CH}_3\text{OH}$ ) ices (Hudson & Moore 2000; Öberg et al. 2009). Interestingly, the  $(\text{CH}_2\text{OH})_2/\text{CH}_2\text{OHCHO}$  abundance ratio is found to be dependent on the initial ice composition as well as the ice temperature during the UV irradiation. The  $\text{CH}_3\text{OH}:\text{CO}$  ratio in the ices is a key parameter: for irradiated 20 K ices a composition of pure  $\text{CH}_3\text{OH}$  leads to a  $(\text{CH}_2\text{OH})_2/\text{CH}_2\text{OHCHO}$  ratio higher than 10, while a  $\text{CH}_3\text{OH}:\text{CO}$  1:10 ice mixture produces a  $(\text{CH}_2\text{OH})_2/\text{CH}_2\text{OHCHO}$  ratio lower than 0.25 (Öberg et al. 2009). The difference found between IRAS16293 and IRAS2A could then be related to a different grain mantle composition in the two sources. If the  $\text{CH}_3\text{OH}:\text{CO}$  ratio in the grain mantles of IRAS 2A was higher than in IRAS 16293, a higher  $(\text{CH}_2\text{OH})_2/\text{CH}_2\text{OHCHO}$  abundance ratio would be expected according to the laboratory results. In fact, the  $\text{CH}_3\text{OH}$  gas-phase abundance in the inner envelope is found to be higher in IRAS2A ( $\sim 4 \times 10^{-7}$ , Jørgensen et al. 2005b) than in IRAS16293 ( $\sim 1 \times 10^{-7}$ , Schöier et al. 2002), while the CO abundance is relatively similar ( $\sim (2\text{--}3) \times 10^{-5}$ , Jørgensen et al. 2002; Schöier et al. 2002). This could consequently be the result of the desorption of ices with a higher  $\text{CH}_3\text{OH}:\text{CO}$  ratio in IRAS2A than IRAS16293. The question then arises: how can  $\text{CH}_3\text{OH}$  be more efficiently produced on grains in IRAS2A than in IRAS16293? Several scenarios are possible: *i)* The initial conditions may play an important role in the  $\text{CH}_3\text{OH}:\text{CO}$  ratio. In particular, experiments and simulations show that the efficiency of  $\text{CH}_3\text{OH}$  formation through CO hydrogenation on the grains is dependent on temperature, ice composition ( $\text{CO}:\text{H}_2\text{O}$ ), and time (Watanabe et al. 2004; Fuchs et al. 2009). *ii)* The collapse timescale

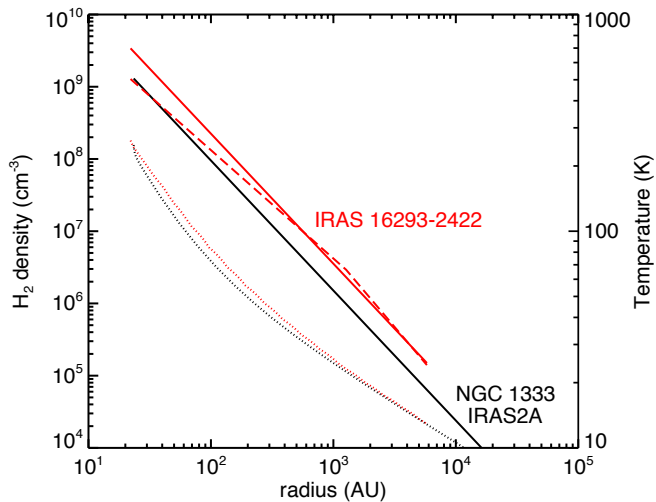


**Fig. 5.** Black:  $\text{H}_2$  density (solid line) and temperature (dotted line) profiles of the protostar IRAS2A from Jørgensen et al. (2002). Red:  $\text{H}_2$  density (solid line: power-law model, dashed line: Shu-like model) and temperature (dotted line) profiles of the protostar IRAS16293 from Crimier et al. (2010).

was longer in IRAS2A than in IRAS16293, enabling to form more  $\text{CH}_3\text{OH}$ . *iii*) The  $\text{H}_2$  density in the prestellar envelope of IRAS2A was lower than that of IRAS16293. Indeed a less dense environment would lead to a higher atomic H density and consequently to a higher efficiency of CO hydrogenation. This was proposed by Maret et al. (2004) and Bottinelli et al. (2007) to explain an anti-correlation found between the inner abundances of  $\text{H}_2\text{CO}$  and  $\text{CH}_3\text{OH}$  and the submillimeter luminosity to bolometric luminosity ( $L_{\text{submm}}/L_{\text{bol}}$ ) ratios of different low-mass protostars. The  $L_{\text{submm}}/L_{\text{bol}}$  parameter is interpreted as an indication of different initial conditions, rather than an evolutionary parameter in this context (Maret et al. 2004). The  $L_{\text{submm}}/L_{\text{bol}}$  ratios of IRAS2A ( $\sim 0.005$ , Karska et al. 2013) and IRAS16293 ( $\sim 0.019$ , Froebrich 2005) are consistent with this hypothesis. The current  $\text{H}_2$  density profiles of these two sources are also in agreement with this scenario, if they keep the memory of the prestellar conditions. The density derived in the outer envelope of IRAS2A with a power-law model (Jørgensen et al. 2002) is lower than the density derived in IRAS16293 by Crimier et al. (2010) whether it be for a Shu-like model or a power-law model, while the temperature profiles are relatively similar (see Figure 5). Along the same lines, Hudson et al. (2005) showed with proton irradiation experiments that glycolaldehyde is more sensitive to radiation damage than ethylene glycol. Irradiation would be more important in less dense envelopes, which would also be consistent with a less dense prestellar envelope in IRAS2A. A recent experiment by Fedoseev et al. (submitted) shows that these two species can also be synthesized by surface hydrogenations of CO molecules in dense molecular cloud conditions. They do not directly form from  $\text{CH}_3\text{OH}$ , but the results of this experiment show that similarly to  $\text{CH}_3\text{OH}$  that results from successive hydrogenations of CO, ethylene glycol forms by two successive hydrogenations of glycolaldehyde. This is consequently in agreement with the proposed scenario.

In conclusion, the  $(\text{CH}_2\text{OH})_2/\text{CH}_2\text{OHCHO}$  abundance ratio measured in low-mass protostars can be different from one source to another, and possibly consistent with cometary values. In some cases, the  $(\text{CH}_2\text{OH})_2/\text{CH}_2\text{OHCHO}$  ratios determined in comets could consequently be inherited from early stages of star

formation. Such a difference between low-mass protostars could be related to a different  $\text{CH}_3\text{OH}:\text{CO}$  ratio in the grain mantles. A more efficient hydrogenation (due for example to a lower density) on the grains would lead to higher abundances of  $\text{CH}_3\text{OH}$  and  $(\text{CH}_2\text{OH})_2$ . A determination of  $(\text{CH}_2\text{OH})_2/\text{CH}_2\text{OHCHO}$  ratios in larger samples of star-forming regions could help understand how the initial conditions (density, molecular cloud, ...) affect their relative abundances.

**Acknowledgements.** The authors are grateful to the IRAM staff, especially Tessel van der Laan, Arancha Castro-Carrizo, Chin-Shin Chang, and Sabine König, for their help with the calibration of the data. This research was supported by a Junior Group Leader Fellowship from the Lundbeck Foundation (to J.K.). Centre for Star and Planet Formation is funded by the Danish National Research Foundation. MVP acknowledges EU FP7 grant 291141 CHEMPLAN. The research leading to these results has received funding from the European Commission Seventh Framework Programme (FP/2007-2013) under grant agreement N° 283393 (RadioNet3).

## References

- Belloche, A., Müller, H. S. P., Menten, K. M., Schilke, P., & Comito, C. 2013, *A&A*, 559, A47
- Beltrán, M. T., Codella, C., Viti, S., Neri, R., & Cesaroni, R. 2009, *ApJ*, 690, L93
- Bisschop, S. E., Jørgensen, J. K., Bourke, T. L., Bottinelli, S., & van Dishoeck, E. F. 2008, *A&A*, 488, 959
- Biver, N., Bockelée-Morvan, D., Debout, V., et al. 2014, *A&A*, 566, L5
- Bottinelli, S., Ceccarelli, C., Neri, R., et al. 2004a, *ApJ*, 617, L69
- Bottinelli, S., Ceccarelli, C., Lefloch, B., et al. 2004b, *ApJ*, 615, 354
- Bottinelli, S., Ceccarelli, C., Williams, J. P., & Lefloch, B. 2007, *A&A*, 463, 601
- Butler, R. A. H., De Lucia, F. C., Petkie, D. T., et al. 2001, *ApJS*, 134, 319
- Carroll, P. B., Drouin, B. J., & Widicus Weaver, S. L. 2010, *ApJ*, 723, 845
- Cazaux, S., Tielens, A. G. G. M., Ceccarelli, C., et al. 2003, *ApJ*, 593, L51
- Ceccarelli, C. 2004, *Star Formation in the Interstellar Medium: In Honor of David Hollenbach*, 323, 195
- Christen, D., Müller, H. S. P. 2003, *Physical Chemistry Chemical Physics (Incorporating Faraday Transactions)*, 5, 3600
- Christen, D., Coudert, L. H., Suenram, R. D., & Lovas, F. J. 1995, *Journal of Molecular Spectroscopy*, 172, 57
- Cooper, G., Kimmich, N., Belisle, W., et al. 2001, *Nature*, 414, 879
- Coutens, A., Jørgensen, J. K., Persson, M. V., et al. 2014, *ApJ*, 792, L5
- Crimier, N., Ceccarelli, C., Maret, S., et al. 2010, *A&A*, 519, A65
- Crovisier, J., Bockelée-Morvan, D., Biver, N., et al. 2004, *A&A*, 418, L35
- Fedoseev, G., Cupper H. M., Ioppolo, S., Lamberts, T. & Linnartz, H., submitted to *MNRAS*
- Froebrih, D. 2005, *ApJS*, 156, 169
- Fuchs, G. W., Cuppen, H. M., Ioppolo, S., et al. 2009, *A&A*, 505, 629
- Fuente, A., Cernicharo, J., Caselli, P., et al. 2014, *A&A*, 568, A65
- Garrod, R. T., Weaver, S. L. W., & Herbst, E. 2008, *ApJ*, 682, 283
- Garrod, R. T. 2013, *ApJ*, 765, 60
- Goldsmith, P. F., & Langer, W. D. 1999, *ApJ*, 517, 209
- Halfen, D. T., Apponi, A. J., Woolf, N., Polt, R., & Ziurys, L. M. 2006, *ApJ*, 639, 237
- Herbst, E., & van Dishoeck, E. F. 2009, *ARA&A*, 47, 427
- Hollis, J. M., Lovas, F. J., & Jewell, P. R. 2000, *ApJ*, 540, L107
- Hollis, J. M., Vogel, S. N., Snyder, L. E., Jewell, P. R., & Lovas, F. J. 2001, *ApJ*, 554, L81
- Hollis, J. M., Lovas, F. J., Jewell, P. R., & Coudert, L. H. 2002, *ApJ*, 571, L59
- Hollis, J. M., Jewell, P. R., Lovas, F. J., & Remijan, A. 2004, *ApJ*, 613, L45
- Hudson, R. L., & Moore, M. H. 2000, *Icarus*, 145, 661
- Hudson, R. L., Moore, M. H., & Cook, A. M. 2005, *Advances in Space Research*, 36, 184
- Ilyushin, V., Kryvda, A., & Alekseev, E. 2009, *Journal of Molecular Spectroscopy*, 255, 32
- Jalbout, A. F., Abrell, L., Adamowicz, L., et al. 2007, *Astrobiology*, 7, 433
- Jørgensen, J. K., Schöier, F. L., & van Dishoeck, E. F. 2002, *A&A*, 389, 908
- Jørgensen, J. K., Bourke, T. L., Myers, P. C., et al. 2005a, *ApJ*, 632, 973
- Jørgensen, J. K., Schöier, F. L., & van Dishoeck, E. F. 2005b, *A&A*, 437, 501
- Jørgensen, J. K., Bourke, T. L., Myers, P. C., et al. 2007, *ApJ*, 659, 479
- Jørgensen, J. K., Favre, C., Bisschop, S. E., et al. 2012, *ApJ*, 757, L4
- Karska, A., Herczeg, G. J., van Dishoeck, E. F., et al. 2013, *A&A*, 552, A141
- Maret, S., Ceccarelli, C., Caux, E., et al. 2004, *A&A*, 416, 577
- Maury, A. J., Belloche, A., André, P., et al. 2014, *A&A*, 563, L2
- McCaaffrey, V. P., Zellner, N. E. B., Waun, C. M., Bennett, E. R., & Earl, E. K. 2014, *Origins of Life and Evolution of the Biosphere*, 44, 29

- Müller, H. S. P., Thorwirth, S., Roth, D. A., & Winnewisser, G. 2001, *A&A*, 370, L49
- Müller, H. S. P., & Christen, D. 2004, *Journal of Molecular Spectroscopy*, 228, 298
- Müller, H. S. P., Schlöder, F., Stutzki, J., & Winnewisser, G. 2005, *Journal of Molecular Structure*, 742, 215
- Öberg, K. I., Garrod, R. T., van Dishoeck, E. F., & Linnartz, H. 2009, *A&A*, 504, 891
- Persson, M. V., Jørgensen, J. K., & van Dishoeck, E. F. 2012, *A&A*, 541, AA39
- Persson, M. V., Jørgensen, J. K., van Dishoeck, E. F., & Harsono, D. 2014, *A&A*, 563, A74
- Pickett, H. M., Poynter, R. L., Cohen, E. A., et al. 1998, *J. Quant. Spec. Radiat. Transf.*, 60, 883
- Requena-Torres, M. A., Martín-Pintado, J., Martín, S., & Morris, M. R. 2008, *ApJ*, 672, 352
- Schöier, F. L., Jørgensen, J. K., van Dishoeck, E. F., & Blake, G. A. 2002, *A&A*, 390, 1001
- Widicus Weaver, S. L., Butler, R. A. H., Drouin, B. J., et al. 2005, *ApJS*, 158, 188
- Watanabe, N., Nagaoka, A., Shiraki, T., & Kouchi, A. 2004, *ApJ*, 616, 638
- Woods, P. M., Kelly, G., Viti, S., et al. 2012, *ApJ*, 750, 19
- Woods, P. M., Slater, B., Raza, Z., et al. 2013, *ApJ*, 777, 90
- Zubay, G., & Mui, T. 2001, *Origins of Life and Evolution of the Biosphere*, 31, 87

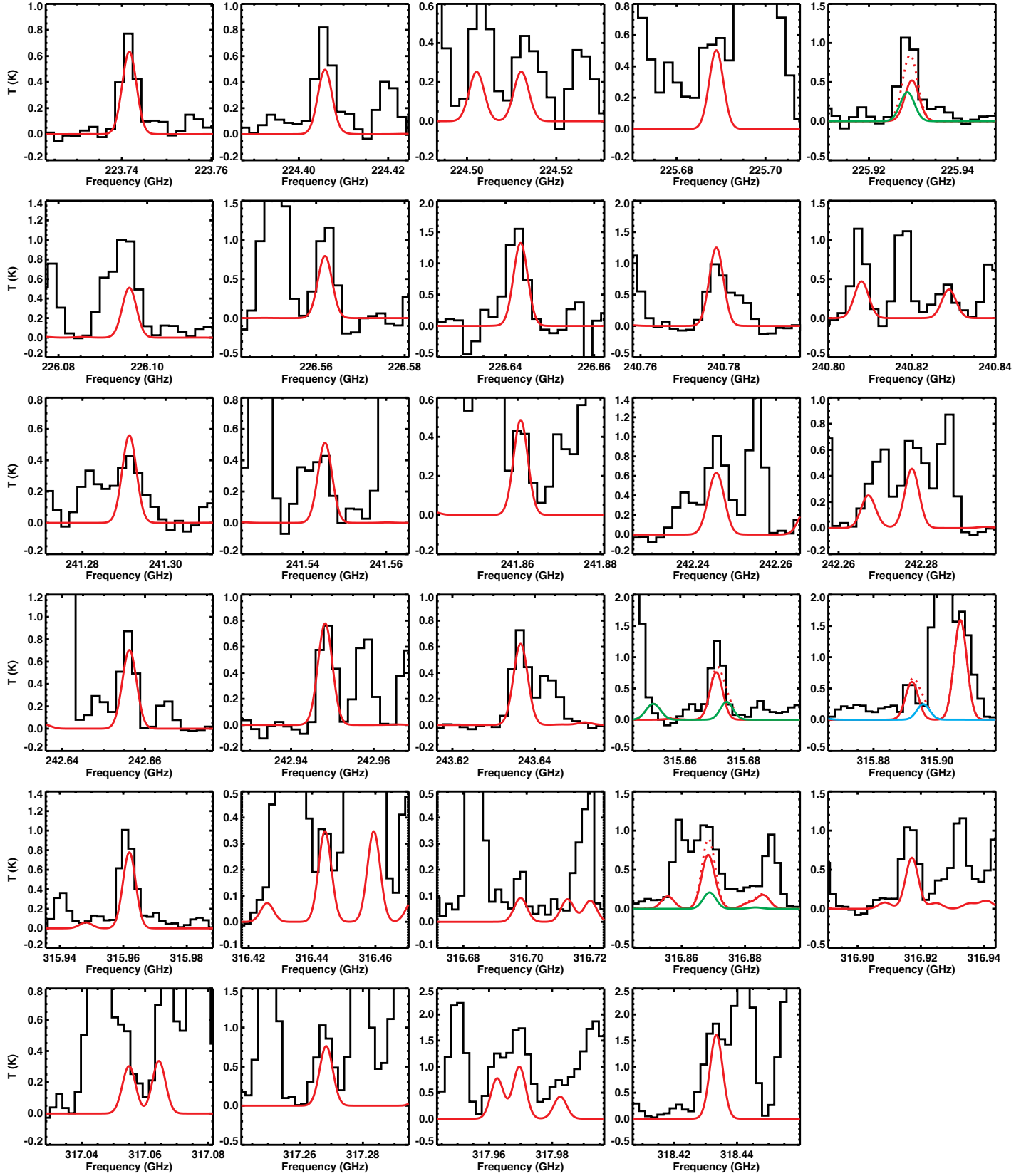


**Fig. 3.** Observed lines of  $\text{aGg}'\text{-(CH}_2\text{OH)}_2$  towards the protostar NGC 1333 IRAS2A (in black). The best-fit model for  $\text{aGg}'\text{-(CH}_2\text{OH)}_2$  (see Table 2) is shown in red solid lines. The contributions of the  $\text{CH}_3\text{OCHO}$  and  $\text{CH}_2\text{OHCHO}$  lines are indicated with green and blue lines, respectively. The model including  $\text{aGg}'\text{-(CH}_2\text{OH)}_2$ ,  $\text{CH}_2\text{OHCHO}$ , and  $\text{CH}_3\text{OCHO}$  can be seen in red dotted lines.



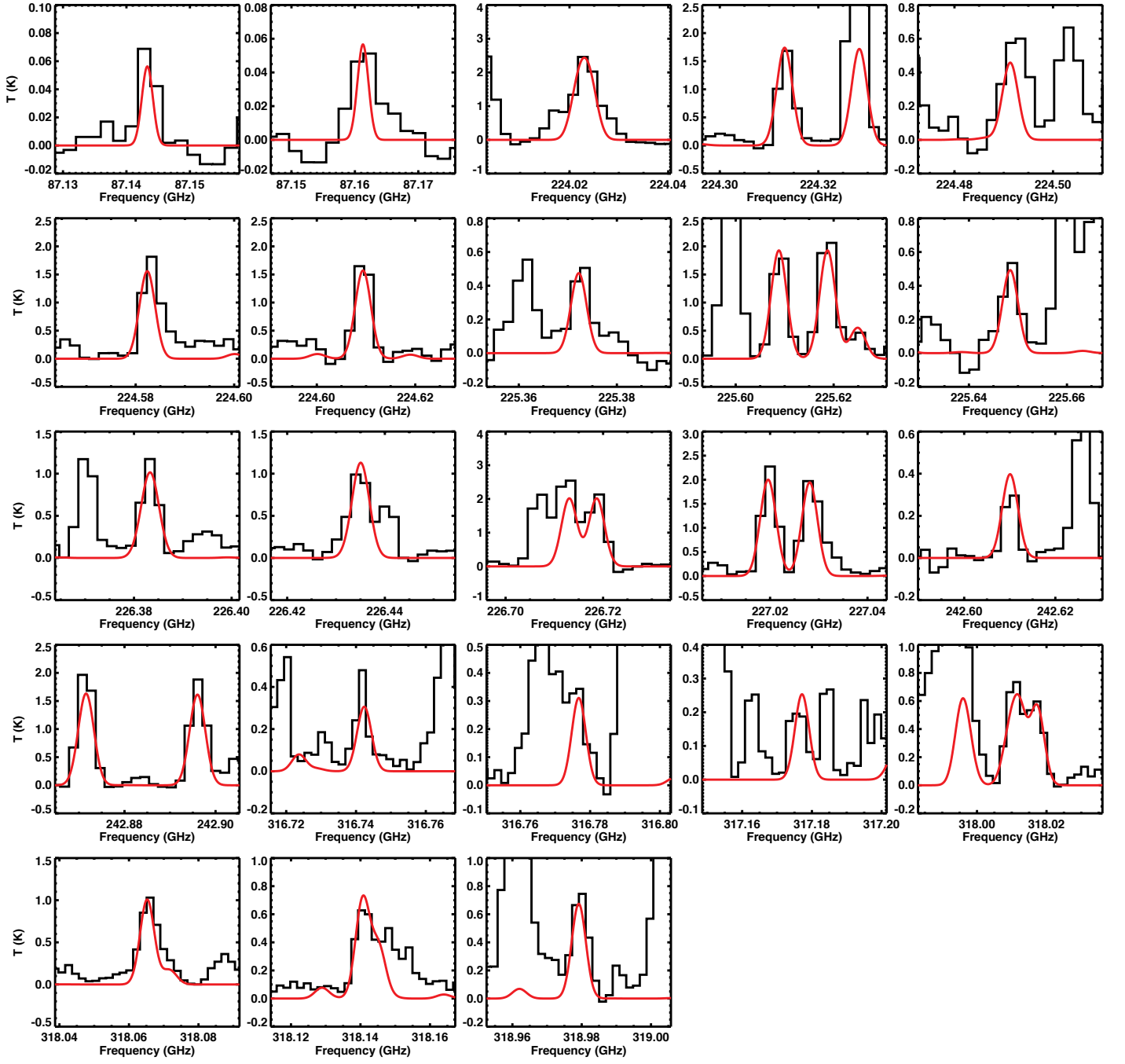


**Fig. 4.** Observed lines of  $\text{CH}_3\text{OCHO}$  towards the protostar NGC 1333 IRAS2A (in black). The best-fit model for  $\text{CH}_3\text{OCHO}$  (see Table 2) is shown in red lines.



**Table 1.** CH<sub>2</sub>OHCHO, aGg'-(CH<sub>2</sub>OH)<sub>2</sub> and CH<sub>3</sub>OCHO transitions observed towards NGC 1333 IRAS2A.

Species	Transition	Frequency (MHz)	$E_{\text{up}}$ (K)	$A_{\text{ij}}$ (s <sup>-1</sup> )	$g_{\text{up}}$	Flux (Jy km s <sup>-1</sup> )	RD <sup>a</sup>
CH <sub>2</sub> OHCHO	13 <sub>10,3</sub> –13 <sub>9,4</sub> ( $v=0$ )	240366.34*	111.3	$1.2 \times 10^{-4}$	27	0.055	Y
	13 <sub>10,4</sub> –13 <sub>9,5</sub> ( $v=0$ )	240366.34*	111.3	$1.2 \times 10^{-4}$	27		
CH <sub>2</sub> OHCHO	12 <sub>10,2</sub> –12 <sub>9,3</sub> ( $v=0$ )	240482.78*	104.0	$1.0 \times 10^{-4}$	25	0.038	Y
	12 <sub>10,3</sub> –12 <sub>9,4</sub> ( $v=0$ )	240482.78*	104.0	$1.0 \times 10^{-4}$	25		
CH <sub>2</sub> OHCHO	11 <sub>5,6</sub> –10 <sub>4,7</sub> ( $v=0$ )	240890.46	51.9	$1.8 \times 10^{-4}$	23	0.663	N <sup>b</sup>
CH <sub>2</sub> OHCHO	22 <sub>2,20</sub> –21 <sub>3,19</sub> ( $v=0$ )	241131.84	142.8	$2.8 \times 10^{-4}$	45	0.061	Y
CH <sub>2</sub> OHCHO	23 <sub>2,22</sub> –22 <sub>1,21</sub> ( $v=0$ )	242239.09	146.2	$3.5 \times 10^{-4}$	47	0.128	Y
CH <sub>2</sub> OHCHO	24 <sub>0,24</sub> –23 <sub>1,23</sub> ( $v=0$ )	242957.72*	148.2	$4.2 \times 10^{-4}$	49	0.258	Y
	24 <sub>1,24</sub> –23 <sub>0,23</sub> ( $v=0$ )	242957.98*	148.2	$4.2 \times 10^{-4}$	49		
CH <sub>2</sub> OHCHO	19 <sub>13,7</sub> –19 <sub>12,8</sub> ( $v=0$ )	315941.48*	208.1	$3.2 \times 10^{-4}$	39	0.074	Y
	19 <sub>13,6</sub> –19 <sub>12,7</sub> ( $v=0$ )	315941.48*	208.1	$3.2 \times 10^{-4}$	39		
CH <sub>2</sub> OHCHO	11 <sub>8,4</sub> –10 <sub>7,3</sub> ( $v=0$ )	317013.88*	75.5	$6.6 \times 10^{-4}$	23	0.363	Y <sup>c</sup>
	11 <sub>8,3</sub> –10 <sub>7,4</sub> ( $v=0$ )	317013.90*	75.5	$6.6 \times 10^{-4}$	23		
CH <sub>2</sub> OHCHO	27 <sub>5,23</sub> –26 <sub>4,22</sub> ( $v=0$ )	317850.44	226.2	$4.5 \times 10^{-4}$	55	0.117	Y <sup>c</sup>
aGg'-(CH <sub>2</sub> OH) <sub>2</sub>	21 <sub>6,16</sub> ( $v=1$ )–20 <sub>6,15</sub> ( $v=0$ )	223741.66	132.0	$2.5 \times 10^{-4}$	387	0.212	Y
aGg'-(CH <sub>2</sub> OH) <sub>2</sub>	21 <sub>6,15</sub> ( $v=1$ )–20 <sub>6,14</sub> ( $v=0$ )	224405.85	132.1	$2.5 \times 10^{-4}$	301	0.197	Y
aGg'-(CH <sub>2</sub> OH) <sub>2</sub>	24 <sub>0,24</sub> ( $v=1$ )–23 <sub>1,23</sub> ( $v=0$ )	224511.70*	136.8	$5.4 \times 10^{-5}$	441	0.145	N
	24 <sub>1,24</sub> ( $v=1$ )–23 <sub>0,23</sub> ( $v=0$ )	224512.74*	136.8	$5.4 \times 10^{-5}$	343		
aGg'-(CH <sub>2</sub> OH) <sub>2</sub>	21 <sub>3,18</sub> ( $v=1$ )–20 <sub>3,17</sub> ( $v=0$ )	225688.94	121.3	$2.4 \times 10^{-4}$	301	0.195	Y
aGg'-(CH <sub>2</sub> OH) <sub>2</sub>	22 <sub>3,20</sub> ( $v=1$ )–21 <sub>3,19</sub> ( $v=0$ )	225929.69	127.8	$2.5 \times 10^{-4}$	315	0.349	N <sup>c</sup>
aGg'-(CH <sub>2</sub> OH) <sub>2</sub>	22 <sub>5,17</sub> ( $v=0$ )–21 <sub>5,16</sub> ( $v=1$ )	226095.96	138.2	$2.6 \times 10^{-4}$	315	0.303	N
aGg'-(CH <sub>2</sub> OH) <sub>2</sub>	22 <sub>2,20</sub> ( $v=1$ )–21 <sub>2,19</sub> ( $v=0$ )	226561.99	127.7	$3.0 \times 10^{-4}$	405	0.329	Y
aGg'-(CH <sub>2</sub> OH) <sub>2</sub>	25 <sub>1,25</sub> ( $v=0$ )–24 <sub>1,24</sub> ( $v=1$ )	226643.30*	147.7	$2.9 \times 10^{-4}$	357	0.470	Y
	25 <sub>0,25</sub> ( $v=0$ )–24 <sub>0,24</sub> ( $v=1$ )	226643.46*	147.7	$2.9 \times 10^{-4}$	459		
aGg'-(CH <sub>2</sub> OH) <sub>2</sub>	25 <sub>1,25</sub> ( $v=1$ )–24 <sub>1,24</sub> ( $v=0$ )	240778.12*	148.0	$3.4 \times 10^{-4}$	459	0.360	Y
	25 <sub>0,25</sub> ( $v=1$ )–24 <sub>0,24</sub> ( $v=0$ )	240778.30*	148.0	$3.4 \times 10^{-4}$	357		
aGg'-(CH <sub>2</sub> OH) <sub>2</sub>	24 <sub>8,17</sub> ( $v=0$ )–23 <sub>8,16</sub> ( $v=1$ )	240807.88	179.2	$3.0 \times 10^{-4}$	441	0.340	N <sup>e</sup>
aGg'-(CH <sub>2</sub> OH) <sub>2</sub>	24 <sub>8,16</sub> ( $v=0$ )–23 <sub>8,15</sub> ( $v=1$ )	240828.89	179.2	$3.0 \times 10^{-4}$	343	0.149	Y
aGg'-(CH <sub>2</sub> OH) <sub>2</sub>	24 <sub>5,20</sub> ( $v=0$ )–23 <sub>5,19</sub> ( $v=1$ )	241291.27	160.7	$3.1 \times 10^{-4}$	441	0.196	Y
aGg'-(CH <sub>2</sub> OH) <sub>2</sub>	24 <sub>7,18</sub> ( $v=0$ )–23 <sub>7,17</sub> ( $v=1$ )	241545.26	172.1	$3.1 \times 10^{-4}$	441	0.151	Y
aGg'-(CH <sub>2</sub> OH) <sub>2</sub>	24 <sub>6,19</sub> ( $v=0$ )–23 <sub>6,18</sub> ( $v=1$ )	241860.73	166.0	$2.8 \times 10^{-4}$	441	0.137	Y
aGg'-(CH <sub>2</sub> OH) <sub>2</sub>	23 <sub>15,8</sub> ( $v=1$ )–22 <sub>15,7</sub> ( $v=0$ )	242244.69*	246.4	$2.0 \times 10^{-4}$	329	0.474	N
	23 <sub>15,9</sub> ( $v=1$ )–22 <sub>15,8</sub> ( $v=0$ )	242244.69*	246.4	$2.0 \times 10^{-4}$	423		
	23 <sub>6,17</sub> ( $v=1$ )–22 <sub>6,17</sub> ( $v=1$ )	242245.62*	154.6	$1.1 \times 10^{-5}$	329		
	23 <sub>14,9</sub> ( $v=1$ )–22 <sub>14,8</sub> ( $v=0$ )	242246.34*	232.2	$2.2 \times 10^{-4}$	329		
	23 <sub>14,10</sub> ( $v=1$ )–22 <sub>14,9</sub> ( $v=0$ )	242246.34*	232.2	$2.2 \times 10^{-4}$	423		
aGg'-(CH <sub>2</sub> OH) <sub>2</sub>	23 <sub>13,10</sub> ( $v=1$ )–22 <sub>13,9</sub> ( $v=0$ )	242277.72*	218.9	$2.4 \times 10^{-4}$	329	0.275	N
	23 <sub>13,11</sub> ( $v=1$ )–22 <sub>13,10</sub> ( $v=0$ )	242277.72*	218.9	$2.4 \times 10^{-4}$	423		
aGg'-(CH <sub>2</sub> OH) <sub>2</sub>	23 <sub>10,14</sub> ( $v=1$ )–22 <sub>10,13</sub> ( $v=0$ )	242656.22*	185.2	$2.8 \times 10^{-4}$	423	0.305	Y
	23 <sub>10,13</sub> ( $v=1$ )–22 <sub>10,12</sub> ( $v=0$ )	242656.24*	185.2	$2.8 \times 10^{-4}$	329		
aGg'-(CH <sub>2</sub> OH) <sub>2</sub>	23 <sub>9,15</sub> ( $v=1$ )–22 <sub>9,14</sub> ( $v=0$ )	242947.99*	175.9	$3.0 \times 10^{-4}$	423	0.291	Y
	23 <sub>9,14</sub> ( $v=1$ )–22 <sub>9,13</sub> ( $v=0$ )	242948.59*	175.9	$3.0 \times 10^{-4}$	329		
aGg'-(CH <sub>2</sub> OH) <sub>2</sub>	23 <sub>5,19</sub> ( $v=1$ )–22 <sub>5,18</sub> ( $v=0$ )	243636.57*	149.1	$3.4 \times 10^{-4}$	423	0.287	Y
aGg'-(CH <sub>2</sub> OH) <sub>2</sub>	31 <sub>8,23</sub> ( $v=0$ )–30 <sub>8,22</sub> ( $v=1$ )	315671.33	276.6	$7.0 \times 10^{-4}$	567	0.314	N <sup>c</sup>
aGg'-(CH <sub>2</sub> OH) <sub>2</sub>	31 <sub>7,25</sub> ( $v=0$ )–30 <sub>7,24</sub> ( $v=1$ )	315892.11	269.6	$6.8 \times 10^{-4}$	441	0.144	N <sup>d</sup>
aGg'-(CH <sub>2</sub> OH) <sub>2</sub>	30 <sub>9,21</sub> ( $v=1$ )–29 <sub>9,20</sub> ( $v=0$ )	315961.89	269.4	$7.0 \times 10^{-4}$	549	0.259	Y
aGg'-(CH <sub>2</sub> OH) <sub>2</sub>	34 <sub>1,34</sub> ( $v=0$ )–33 <sub>0,33</sub> ( $v=0$ )	316444.07*	268.5	$1.6 \times 10^{-4}$	621	0.078	Y
	34 <sub>0,34</sub> ( $v=0$ )–33 <sub>1,33</sub> ( $v=0$ )	316444.07*	268.5	$1.6 \times 10^{-4}$	483		
aGg'-(CH <sub>2</sub> OH) <sub>2</sub>	20 <sub>6,14</sub> ( $v=0$ )–19 <sub>5,15</sub> ( $v=0$ )	316698.08	121.3	$5.1 \times 10^{-5}$	287	0.029	Y
aGg'-(CH <sub>2</sub> OH) <sub>2</sub>	30 <sub>7,24</sub> ( $v=1$ )–29 <sub>7,23</sub> ( $v=0$ )	316868.23*	254.4	$6.9 \times 10^{-4}$	427	0.445	N <sup>c</sup>
	20 <sub>16,4</sub> ( $v=0$ )–20 <sub>15,5</sub> ( $v=0$ )	316870.92*	228.9	$3.8 \times 10^{-5}$	287		
	20 <sub>16,5</sub> ( $v=0$ )–20 <sub>15,6</sub> ( $v=0$ )	316870.92*	228.9	$3.8 \times 10^{-5}$	369		
aGg'-(CH <sub>2</sub> OH) <sub>2</sub>	30 <sub>8,23</sub> ( $v=1$ )–29 <sub>8,22</sub> ( $v=0$ )	316917.19	261.4	$7.2 \times 10^{-4}$	427	0.299	Y
aGg'-(CH <sub>2</sub> OH) <sub>2</sub>	16 <sub>8,9</sub> ( $v=1$ )–15 <sub>7,8</sub> ( $v=1$ )	317054.30*	98.6	$8.0 \times 10^{-5}$	231	0.116	N
	16 <sub>8,8</sub> ( $v=1$ )–15 <sub>7,9</sub> ( $v=1$ )	317055.36*	98.6	$8.0 \times 10^{-5}$	297		
aGg'-(CH <sub>2</sub> OH) <sub>2</sub>	21 <sub>4,18</sub> ( $v=1$ )–20 <sub>4,18</sub> ( $v=0$ )	317267.77*	122.1	$1.1 \times 10^{-5}$	387	0.312	N

	14 <sub>9,5</sub> ( $v=1$ )–13 <sub>8,6</sub> ( $v=1$ )	317267.91*	91.4	$1.1 \times 10^{-4}$	261		
	14 <sub>9,6</sub> ( $v=1$ )–13 <sub>8,5</sub> ( $v=1$ )	317267.91*	91.4	$1.1 \times 10^{-4}$	203		
	14 <sub>9,5</sub> ( $v=0$ )–13 <sub>8,6</sub> ( $v=0$ )	317268.88*	91.4	$1.1 \times 10^{-4}$	203		
	14 <sub>9,6</sub> ( $v=0$ )–13 <sub>8,5</sub> ( $v=0$ )	317268.88*	91.4	$1.1 \times 10^{-4}$	261		
aGg'-(CH <sub>2</sub> OH) <sub>2</sub>	32 <sub>3,30</sub> ( $v=1$ )–31 <sub>3,29</sub> ( $v=0$ )	317962.58	257.2	$7.8 \times 10^{-4}$	455	0.310	Y
aGg'-(CH <sub>2</sub> OH) <sub>2</sub>	32 <sub>4,28</sub> ( $v=0$ )–31 <sub>4,27</sub> ( $v=1$ )	317982.56	272.2	$4.8 \times 10^{-4}$	455	0.160	Y
aGg'-(CH <sub>2</sub> OH) <sub>2</sub>	35 <sub>0,35</sub> ( $v=0$ )–34 <sub>0,34</sub> ( $v=1$ )	318433.40*	284.1	$8.0 \times 10^{-4}$	639	0.639	N
	35 <sub>1,35</sub> ( $v=0$ )–34 <sub>1,34</sub> ( $v=1$ )	318433.40*	284.1	$8.0 \times 10^{-4}$	497		
CH <sub>3</sub> OCHO	7 <sub>3,4</sub> –6 <sub>3,3</sub> E ( $v_T=0$ )	87143.28*	22.6	$7.7 \times 10^{-6}$	30	0.049	N
	21 <sub>5,16</sub> –21 <sub>4,17</sub> E ( $v_T=1$ )	87143.65*	342.0	$1.4 \times 10^{-6}$	86		
CH <sub>3</sub> OCHO	8 <sub>0,8</sub> –7 <sub>1,7</sub> E ( $v_T=1$ )	87160.84*	207.0	$1.3 \times 10^{-6}$	34	0.038	N
	7 <sub>3,4</sub> –6 <sub>3,3</sub> A ( $v_T=0$ )	87161.28*	22.6	$7.8 \times 10^{-6}$	30		
CH <sub>3</sub> OCHO	18 <sub>6,13</sub> –17 <sub>6,12</sub> E ( $v_T=0$ )	224021.87*	125.3	$1.5 \times 10^{-4}$	74	0.752	Y
	18 <sub>6,13</sub> –17 <sub>6,12</sub> A ( $v_T=0$ )	224024.10*	125.3	$1.5 \times 10^{-4}$	74		
CH <sub>3</sub> OCHO	18 <sub>5,14</sub> –17 <sub>5,13</sub> E ( $v_T=0$ )	224313.15	118.3	$1.6 \times 10^{-4}$	74	0.351	Y
CH <sub>3</sub> OCHO	19 <sub>3,17</sub> –18 <sub>3,16</sub> E ( $v_T=1$ )	224491.31	303.2	$1.7 \times 10^{-4}$	78	0.212	Y
CH <sub>3</sub> OCHO	18 <sub>6,12</sub> –18 <sub>6,11</sub> E ( $v_T=0$ )	224582.35	125.4	$1.5 \times 10^{-4}$	74	0.463	Y
CH <sub>3</sub> OCHO	18 <sub>6,12</sub> –17 <sub>6,11</sub> A ( $v_T=0$ )	224609.38	125.4	$1.5 \times 10^{-4}$	74	0.466	Y
CH <sub>3</sub> OCHO	20 <sub>2,19</sub> –19 <sub>2,18</sub> A ( $v_T=1$ )	225372.22	307.3	$1.7 \times 10^{-4}$	82	0.186	Y
CH <sub>3</sub> OCHO	19 <sub>3,17</sub> –18 <sub>3,16</sub> E ( $v_T=0$ )	225608.82	116.7	$1.7 \times 10^{-4}$	78	0.426	Y
CH <sub>3</sub> OCHO	18 <sub>5,13</sub> –17 <sub>5,12</sub> A ( $v_T=1$ )	225648.42*	305.6	$1.6 \times 10^{-4}$	74	0.163	N
	26 <sub>9,18</sub> –26 <sub>8,19</sub> A ( $v_T=0$ )	225648.42*	261.7	$1.6 \times 10^{-5}$	106		
CH <sub>3</sub> OCHO	21 <sub>0,21</sub> –20 <sub>1,20</sub> A ( $v_T=1$ )	226381.36*	309.6	$2.8 \times 10^{-5}$	86	0.277	Y
	21 <sub>1,21</sub> –20 <sub>1,20</sub> A ( $v_T=1$ )	226382.72*	309.6	$1.7 \times 10^{-4}$	86		
	21 <sub>0,21</sub> –20 <sub>0,20</sub> A ( $v_T=1$ )	226383.86*	309.6	$1.7 \times 10^{-4}$	86		
	21 <sub>1,21</sub> –20 <sub>0,20</sub> A ( $v_T=1$ )	226385.15*	309.6	$2.8 \times 10^{-5}$	86		
CH <sub>3</sub> OCHO	21 <sub>0,21</sub> –20 <sub>1,20</sub> E ( $v_T=1$ )	226433.26*	308.9	$2.7 \times 10^{-5}$	86	0.296	N
	21 <sub>1,21</sub> –20 <sub>1,20</sub> E ( $v_T=1$ )	226434.47*	308.9	$1.7 \times 10^{-4}$	86		
	21 <sub>0,21</sub> –20 <sub>0,20</sub> E ( $v_T=1$ )	226435.52*	308.9	$1.7 \times 10^{-4}$	86		
	25 <sub>9,16</sub> –25 <sub>8,17</sub> A ( $v_T=0$ )	226435.52*	246.2	$1.6 \times 10^{-5}$	102		
	21 <sub>1,21</sub> –20 <sub>0,20</sub> E ( $v_T=1$ )	226436.66*	308.9	$2.7 \times 10^{-5}$	86		
CH <sub>3</sub> OCHO	20 <sub>2,19</sub> –19 <sub>2,18</sub> A ( $v_T=0$ )	226718.69	120.2	$1.7 \times 10^{-4}$	82	0.505	Y
CH <sub>3</sub> OCHO	19 <sub>2,17</sub> –18 <sub>2,16</sub> E ( $v_T=0$ )	227019.55*	116.6	$1.7 \times 10^{-4}$	78	0.561	N
	25 <sub>9,17</sub> –25 <sub>8,18</sub> A ( $v_T=0$ )	227021.13*	246.2	$1.6 \times 10^{-5}$	102		
CH <sub>3</sub> OCHO	19 <sub>2,17</sub> –18 <sub>2,16</sub> A ( $v_T=0$ )	227028.12	116.6	$1.7 \times 10^{-4}$	78	0.436	Y
CH <sub>3</sub> OCHO	20 <sub>4,17</sub> –19 <sub>4,16</sub> A ( $v_T=1$ )	242610.07	321.7	$2.1 \times 10^{-4}$	82	0.092	Y
CH <sub>3</sub> OCHO	37 <sub>7,31</sub> –37 <sub>6,32</sub> A ( $v_T=0$ )	242870.39*	452.0	$1.8 \times 10^{-5}$	150	0.714	N
	19 <sub>5,14</sub> –18 <sub>5,13</sub> E ( $v_T=0$ )	242871.57*	130.5	$2.0 \times 10^{-4}$	78		
CH <sub>3</sub> OCHO	19 <sub>5,14</sub> –18 <sub>5,13</sub> A ( $v_T=0$ )	242896.02	130.4	$2.0 \times 10^{-4}$	78	0.666	Y
CH <sub>3</sub> OCHO	21 <sub>12,9</sub> –21 <sub>11,10</sub> E ( $v_T=0$ )	316742.00*	231.8	$3.3 \times 10^{-5}$	86	0.072	Y
	21 <sub>12,10</sub> –21 <sub>11,11</sub> E ( $v_T=0$ )	316742.71*	231.8	$3.3 \times 10^{-5}$	86		
CH <sub>3</sub> OCHO	21 <sub>12,9</sub> –21 <sub>11,10</sub> A ( $v_T=0$ )	316776.74*	231.8	$3.3 \times 10^{-5}$	86	0.069	Y
	21 <sub>12,10</sub> –21 <sub>11,11</sub> A ( $v_T=0$ )	316776.74*	231.8	$3.3 \times 10^{-5}$	86		
CH <sub>3</sub> OCHO	26 <sub>13,13</sub> –25 <sub>13,12</sub> E ( $v_T=1$ )	317177.16	506.5	$3.6 \times 10^{-4}$	106	0.043	Y
CH <sub>3</sub> OCHO	9 <sub>8,2</sub> –8 <sub>7,1</sub> A ( $v_T=1$ )	318009.06*	256.8	$6.8 \times 10^{-5}$	38	0.200	N
	9 <sub>8,1</sub> –8 <sub>7,2</sub> A ( $v_T=1$ )	318009.06*	256.8	$6.9 \times 10^{-5}$	38		
	13 <sub>12,1</sub> –13 <sub>11,2</sub> E ( $v_T=0$ )	318009.55*	149.2	$1.3 \times 10^{-5}$	54		
	26 <sub>13,13</sub> –25 <sub>13,12</sub> A ( $v_T=1$ )	318012.17*	506.2	$3.7 \times 10^{-4}$	106		
	26 <sub>13,14</sub> –25 <sub>13,13</sub> A ( $v_T=1$ )	318012.17*	506.2	$3.7 \times 10^{-4}$	106		
CH <sub>3</sub> OCHO	13 <sub>12,2</sub> –13 <sub>11,3</sub> E ( $v_T=0$ )	318016.90*	149.2	$1.3 \times 10^{-5}$	54	0.155	N
	9 <sub>8,1</sub> –8 <sub>7,1</sub> E ( $v_T=0$ )	318017.37*	69.0	$6.7 \times 10^{-5}$	38		
CH <sub>3</sub> OCHO	12 <sub>12,0</sub> –12 <sub>11,1</sub> E ( $v_T=0$ )	318064.54*	141.6	$7.0 \times 10^{-6}$	50	0.204	N
	9 <sub>8,2</sub> –8 <sub>7,1</sub> A ( $v_T=0$ )	318065.26*	69.0	$6.8 \times 10^{-5}$	38		
	9 <sub>8,1</sub> –8 <sub>7,2</sub> A ( $v_T=0$ )	318065.26*	69.0	$6.8 \times 10^{-5}$	38		
CH <sub>3</sub> OCHO	27 <sub>4,23</sub> –26 <sub>5,22</sub> E ( $v_T=1$ )	318139.11*	426.4	$3.4 \times 10^{-5}$	110	0.192	N
	25 <sub>6,19</sub> –24 <sub>6,18</sub> A ( $v_T=1$ )	318140.72*	405.1	$4.6 \times 10^{-4}$	102		
	26 <sub>11,15</sub> –25 <sub>11,14</sub> E ( $v_T=1$ )	318145.25*	474.5	$4.0 \times 10^{-4}$	106		
CH <sub>3</sub> OCHO	27 <sub>4,24</sub> –26 <sub>4,23</sub> E ( $v_T=1$ )	318979.14	417.8	$4.8 \times 10^{-4}$	110	0.208	Y

Notes: The symbol \* present after some frequency values indicates that the associated transition is blended with one or more transitions from the same species. "Y" indicates that the line was considered in the rotational diagram analysis, while N indicates

that it could not be used (for blending reasons). <sup>b</sup>Blended with an unidentified species. <sup>c</sup>Blended with CH<sub>3</sub>OCHO. <sup>d</sup>Blended with CH<sub>2</sub>OHCHO. <sup>e</sup>Potentially blended with the gGg' conformer of ethylene glycol.